Supporting information

for

Robust bifunctionality in oxygen electrode via core-shell heterostructure construction

Yumei Feng[a,b#], Xianwei Li[a,b#], Zhiyong Ma[c], Kaiyi Liu[c], Yi Li[c], Chen Li[a*], Chunsheng Li[d,e], Yan Sun,[d,e*] and Zehui Yang[b*]

[a]State Key Laboratory of New Textile Materials & Advanced Processing Technology, College of Materials Science and Engineering, Wuhan Textile University, Wuhan, 430200, China.

[b]Faculty of Materials Science and Chemistry, China University of Geosciences Wuhan, 388 Lumo RD, Wuhan, 430074, China.

[c]Shaanxi Coal Chemical Industry Technology Research Institute Co., Ltd., Xi'an 710065, China.

[d]School of Chemistry and Life Sciences, Suzhou University of Science and Technology, Suzhou City, Jiangsu Province 215009, China.

[e]Key Laboratory of Advanced Electrode Materials for Novel Solar Cells for Petroleum and Chemical Industry of China, Suzhou University of Science and Technology, Suzhou City, Jiangsu Province 215009, China.

[#]Yumei Feng and Xianwei Li equally contributed to this work.

Experimental section

Materials: Melamine ($C_3H_6N_6$, 99.0%), isopropyl alcohol (C_3H_8O, 99.7%), zinc acetate dihydrate ($C_4H_6O_4Zn{\cdot}2H_2O$, 99.0%), anhydrous methanol (CH_3OH, 99.5%), potassium hydroxide (KOH, 85.0%) and selenium powder (Se, 99.0%) were purchased from Shanghai Sinpharm Chemical Reagent Co. Ltd. Cobalt chloride hexahydrate ($CoCl_2{\cdot}6H_2O$, 99.0%) were acquired from Aladdin Holdings Group. The 5% Nafion solution was purchased from Sigama-Aldrich. The chemical substances involved were directly available at the analytical level. Deionized H_2O was used throughout the experiment.

Synthesis of electrocatalyst: 1.20 g of cobalt chloride ($CoCl_2$) and 6.0 g of melamine ($C_3H_6N_6$) were dissolved in 150 mL of methanol (CH_3OH), stirred and heated at 110 °C for 12 h, and the stirred powder was collected and fully ground and kept in a tube furnace at N_2 atmosphere 800 °C for 2 h. Co@NCNT was obtained. The Co@NCNT was mixed and held at 800 °C for 5 h in a tube furnace (Co@NCNT: Se= 5:1 and 1:1) to obtain Co-CoSe@NCNT and CoSe@NCNT.

Fundamental characterization: The compositional analysis of the synthesized samples were carried out on a Bruker D8 Advance using X-ray diffractometer (XRD) with a scanning rate of 5° min^{-1} and a 2θ range of 5° to 90°. Scanning electron microscopy (SEM) was performed by SU8010. The samples were examined by transmission electron microscopy (TEM), high resolution transmission electron microscopy (HRTEM) and energy spectrometry (EDS) on FEI Talos F200. X-ray photoelectron spectroscopy (XPS) was performed using a Thermo Scientific Escalab

250Xi, and N_2 adsorption-desorption analyses were carried out using an ASAP 2460. The Raman spectra of the samples were obtained using i-Raman Plus.

Oxygen reduction reaction (ORR) test: The ORR performance of the catalysts was tested with a three-electrode system at room temperature. The disk electrode modified with catalyst material was used as the working electrode, the carbon rod electrode and the Hg/HgO electrode were used as the opposite electrode and the reference electrode, respectively. Weighed 4mg catalyst and dispersed it in a 1 mL mixture of 800 μL deionized water, 170 μL isopropyl alcohol and 30 μL 5.0 wt% Nafion, sonicated in an ultrasonic washer for 30 min. The fully dispersed ink solution was dropped on a rotating disk electrode (RDE). The ORR test of the prepared catalyst was carried out in 1 M KOH electrolyte with CHI 760 electrochemical workstation. LSV tests were performed in a 1 M KOH electrolyte saturated with O_2, in the range of 0 to 1.2 V vs. RHE, at a scan rate of 5 mV s^{-1}, and at speeds of 400 rpm, 600 rpm, 800 rpm, 1200 rpm, 1600 rpm, and 2400 rpm.

The electron transfer number was calculated by the following Koutechy-Levich equation:

$$\frac{1}{j} = \frac{1}{j_K} + \frac{1}{j_L} = \frac{1}{B\omega^{1/2}} + \frac{1}{j_K} \quad (1.1)$$

$$B = 0.62\, n\, F\, C_o\, (D_o)^{2/3}\, v^{-1/6} \quad (1.2)$$

$$j_K = n\, F\, k\, C_o \quad (1.3)$$

In the above formula, each symbol is defined as: Test current density (j), diffusion current density (j_L), kinetic limiting current density (j_K), angular velocity (ω), electron transfer number (n), Faraday constant (F), volume concentration of O_2 in electrolyte

(C_o), diffusion coefficient of O_2 in 1 M KOH solution (D_o), dynamic viscosity of electrolyte at room temperature (v), and so on. Electron transfer rate constant (k). At a sweep speed of 100 mV s^{-1}, 5000 cycles CV were performed to evaluate the cyclic durability of the catalyst ORR process.

Oxygen evolution reaction (OER) test: The OER performance was tested in an O_2-saturated 1 M KOH using a Gamry Interface 1000E electrochemical workstation. 5 cycles cyclic voltametric scan (CV) were performed in 1 M KOH to activate the catalyst electrode. Linear sweep voltammetry (LSV) tests were performed in 1 M KOH at a rate of 5 mV s^{-1}.

CV tests were performed on the catalyst at different scan rates (10-100 mV s^{-1}), and the Double-layer capacitance (C_{dl}) was obtained by fitting the catalyst to obtain the electrochemical active surface area (ECSA) of the catalyst: ECSA = C_{dl}/C_s, where C_s was the flat surface specific capacitance value and C_{dl} was the value obtained from the fitting calculation. The frequency range of the electrochemical impedance (EIS) test was set from 100 kHz to 0.1 Hz, and the test voltage was set to correspond to the condition of j=10 mA cm^{-2}.

The electrochemical durability of the catalysts was evaluated by performing CV cycle tests at a sweep rate of 100 mV s^{-1}. And a long-time electrochemical stability test was performed at the potential corresponding to j=10 mA cm^{-2} using timed current test (CA) to evaluate the stability of the catalyst.

Zinc air battery test: The zinc air battery tests were conducted at room temperature. In this case, the liquid ZABs used zinc plates as the anode, catalyst-loaded carbon

paper as the air cathode, a mixture of 6 M KOH and 0.2 M $C_4H_6O_4Zn \cdot 2H_2O$ as the electrolyte, and nickel foam as the collector current signals. The all-solid-state ZABs were basically the same as the liquid battery, except that the all-solid-state ZABs used a KOH doped PVA polymer electrolyte. Specific test methods were as follows：

(1) Open Circuit Voltage test

The Gamry Interface 1000E electrochemical workstation was used to test the open-circuit voltage (OCV) variation of the assembled ZABs.

(2) Charge-discharge curve test

The VMP3B-2x2 electrochemical workstation was used to conduct the charge-discharge tests of ZABs. And the peak power density of discharge was obtained from the discharge curve.

(3) Specific capacity test

Continuous discharge was carried out under the condition of j=5 mA cm^{-2} until the voltage of ZABs dropped to 0 V. The constant current discharge curve was obtained and the specific capacity data was calculated based on the mass of zinc consumed by ZABs:

$$Specificcapacity = \frac{I \times T}{m_{Zn}} \quad (1.4)$$

Where I was the discharge current value (mA), T was the time taken for the battery voltage to drop to 0 V (h), and m_{Zn} was the mass of zinc consumed (g).

(4) Cyclic endurance test

Under the condition of j=5 mA cm^{-2}, the battery was continuously charged for 5 min and then continuously discharged for 5 min as a charge/discharge cycle, and after a

long period of time until the voltage of the battery dropped to 0 V. A long-time charge/discharge cycle curve was obtained to judge the cycle life of the battery.

(5) Constant current charge/discharge test

Charge and discharge the battery continuously for 2 h under the conditions of j=2 mA cm^{-2}, j=5 mA cm^{-2}, j=10 mA cm^{-2} and j=5 mA cm^{-2} in order to obtain the constant current charge/discharge curve to judge the stability of the battery.

DFT calculation: The density functional theory (DFT) analysis was carried out using Vienna Ab-initio Simulation Package (VASP). The exchange–correlation potential was the Perdew–Burke–Ernzerhof (PBE) generalized gradient approximation (GGA) functional. The ion-electron interaction was described by the projected augmented wave (PAW) potential.

According to the HRTEM images, the Co-CoSe@NCNT heterostructure showed an interface between Co (111) surface and CoSe (102) surface. Thus, the interface based on Co (111) and CoSe (102) surfaces was built to simulate the Co-CoSe@NCNT heterostructure. To avoid artificial interactions between periodically repeating plates, the vacuum layer was set to 15 Å.

The cut off energy for the plane-wave base was set to 550 eV, all DFT calculations took spin polarization into account. In the structure optimization, the k-space was sampled with a grid of 3 × 2 × 1, and the state density calculation was 6 × 3 × 1. The convergence criterion of 10^{-5} eV for electron energy and convergence criterion of 10^{-2} eV/Å for the forces on each ion were used to optimize the structures.

The Gibbs free energy changes (ΔG) for each step were determined using the

following equation:

$\Delta G = \Delta E + \Delta ZPE - T\Delta S$

Where ΔE was calculated directly from DFT calculations, ΔZPE was the change in zero-point energies (ZPE), T was the temperature (298.15 K), and ΔS was the change in entropy of products and reactants.

Table S1 Comparison of the battery performances of the reported electrocatalysts.

Catalyst	j ($mA \cdot cm^{-2}$)	Power density ($mW \cdot cm^{-2}$)	Time of cycle life tests (h)	Reference
Co-CoSe@NCNT	5	172	970	This work
Fe_3C/Fe_2O_3@NGN	10	139.8	60	[1]
Co/CoO@FeNC-850	5	132.8	50	[2]
Co-NC@LDH	5	107.8	300	[3]
Co_3O_4@NiFe-LDH	15	127.4	200	[4]
FeNiS-NBC/C	5	133.0	130	[5]
P-CoNi@NSCs	5	87.9	620	[6]
Ni–Co/NFC	20	138.0	200	[7]
TMB@NiNC	10	107.0	230	[8]
Ni_3S_4@CoSx-NF	5	143.0	667	[9]
$Sr_2Fe_{1.5}Mo_{0.5}O_{6-\delta}$	10	137.0	300	[10]
MnOx-FeNi-LDH/NF	10	120	110	[11]
Co-NC@Nb-TiOx	10	123.46	225	[12]

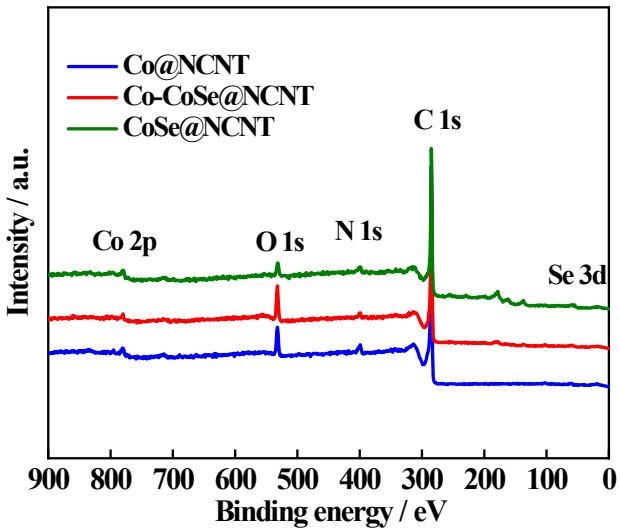

Figure S1 XPS survey scan of Co@NCNT, CoSe@NCNT and Co-CoSe@NCNT.

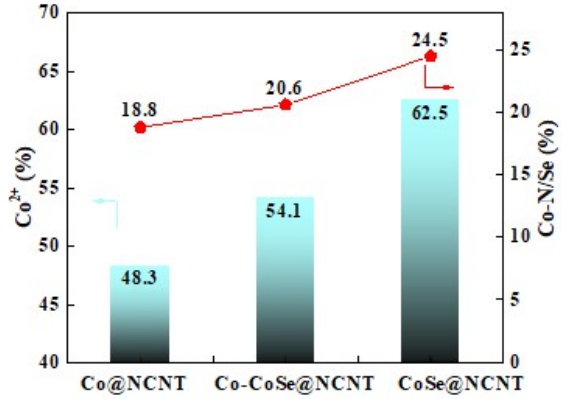

Figure S2 Quantitative analysis of Co 2p peaks of Co@NCNT, CoSe@NCNT and Co-CoSe@NCNT.

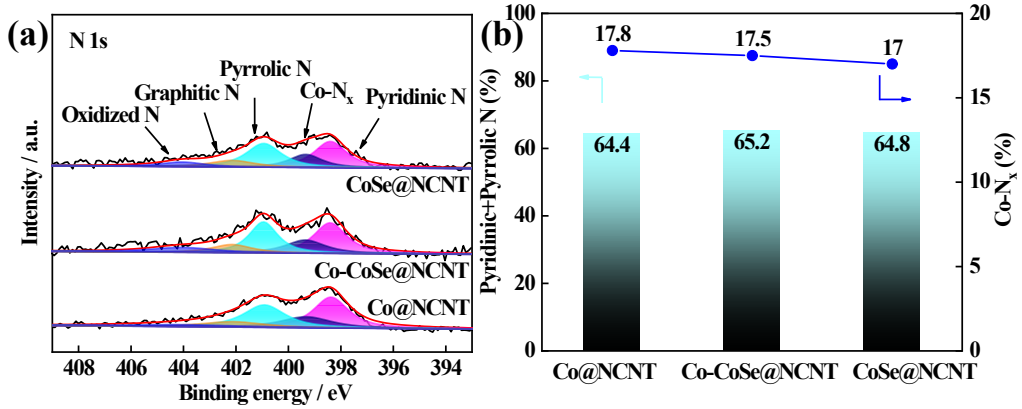

Figure S3 Deconvoluted N 1s peaks of Co@NCNT, CoSe@NCNT and Co-CoSe@NCNT.

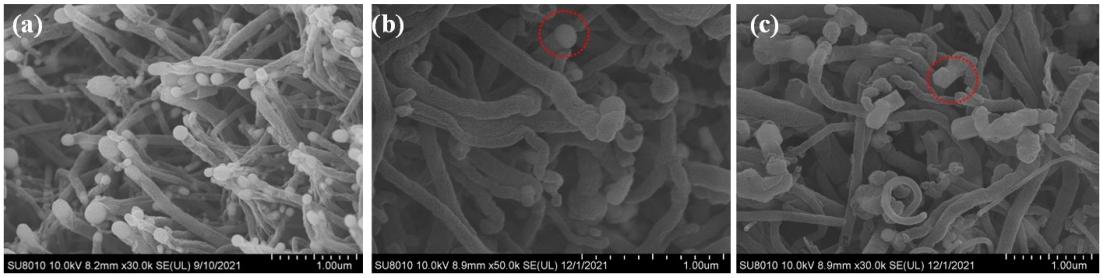

Figure S4 SEM images of Co@NCNT (a), CoSe@NCNT (b) and Co-CoSe@NCNT (c).

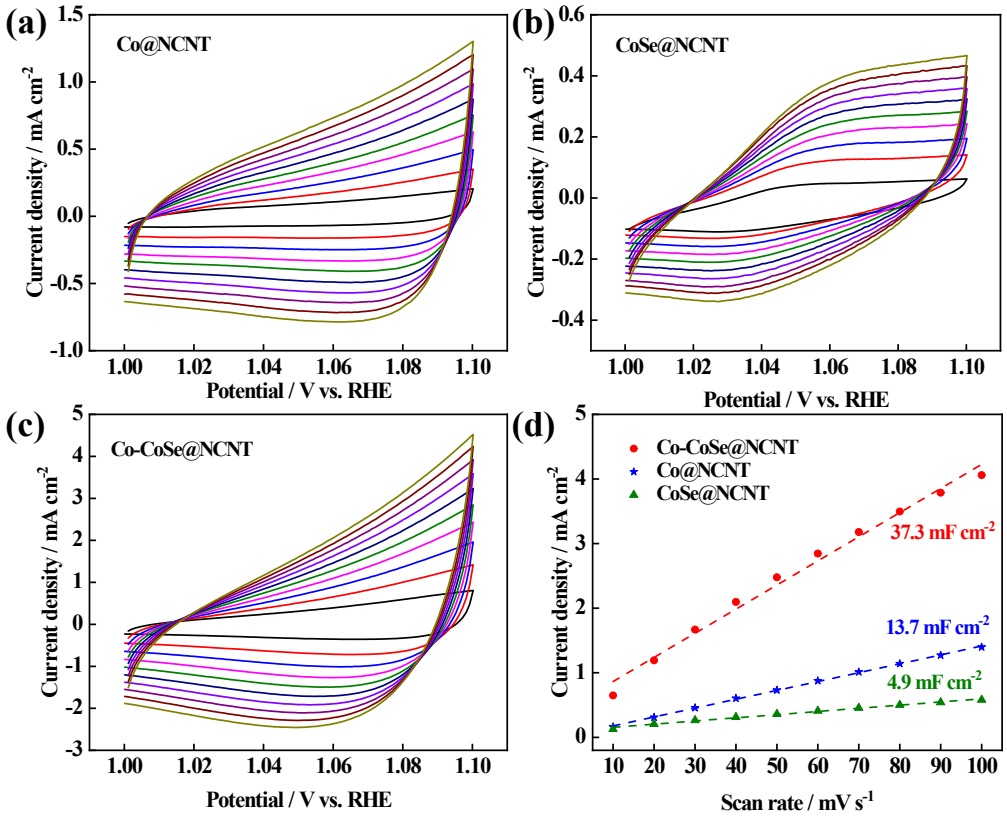

Figure S5 Cyclic voltammetry curves of Co@NCNT (a), CoSe@NCNT (b) and Co-CoSe@NCNT (c). (d) Double layer capacitances of Co@NCNT, CoSe@NCNT and Co-CoSe@NCNT.

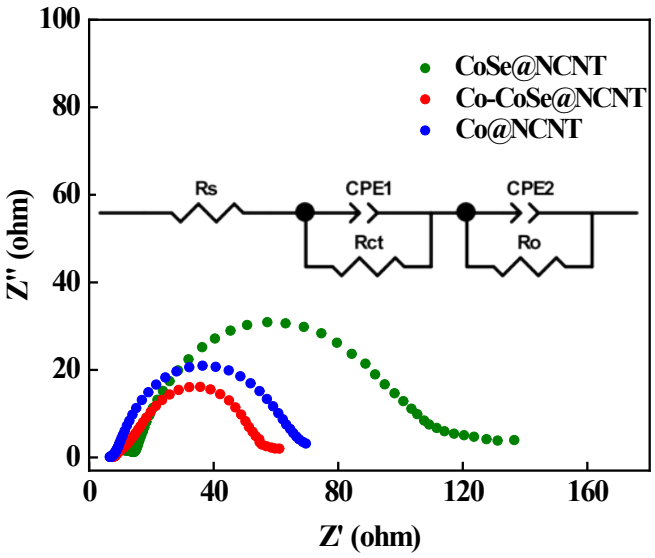

Figure S6 Charge transfer resistance of Co@NCNT, CoSe@NCNT and Co-CoSe@NCNT.

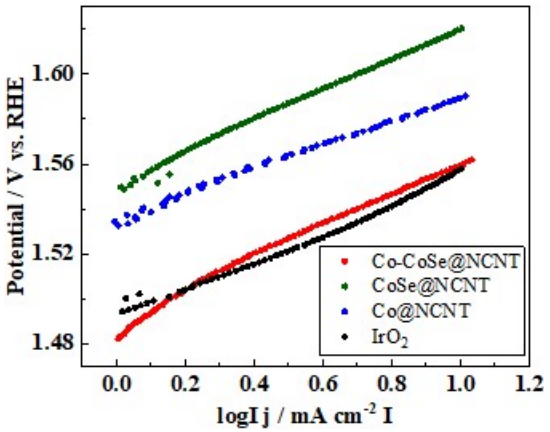

Figure S7 Tafel slopes of IrO_2, Co@NCNT, CoSe@NCNT and Co-CoSe@NCNT.

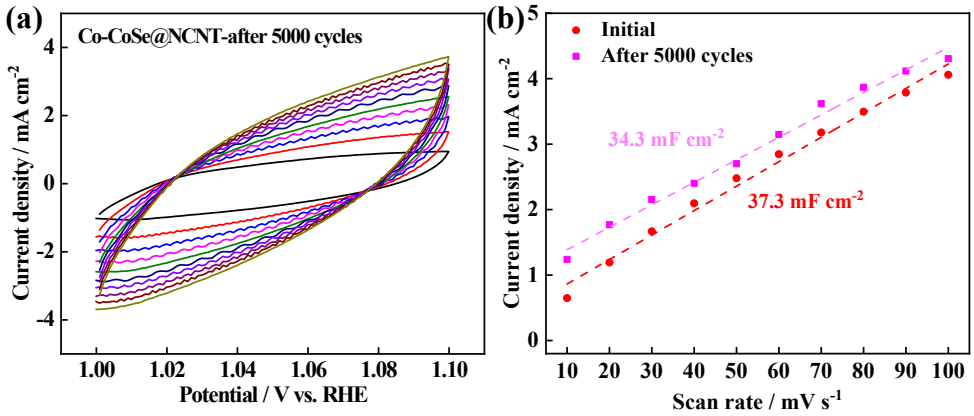

Figure S8 Cyclic voltammetry curves (a) and double layer capacitance (b) of Co-CoSe@NCNT after 5000 cycles.

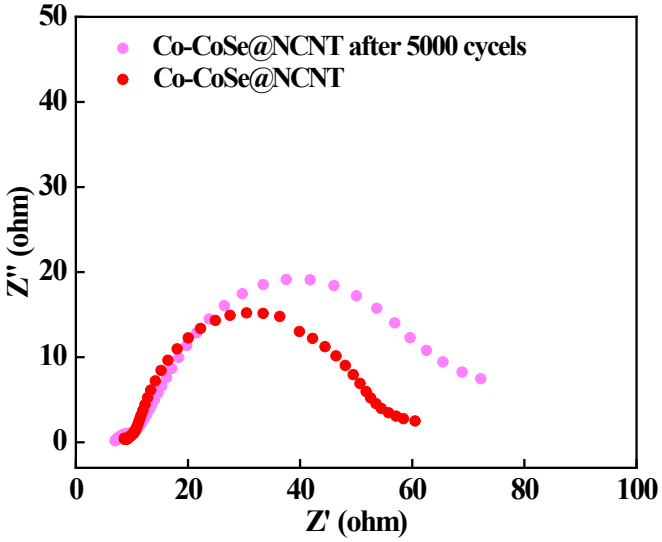

Figure S9 Electrochemical impedance spectroscopy of Co-CoSe@NCNT after 5000 cycles.

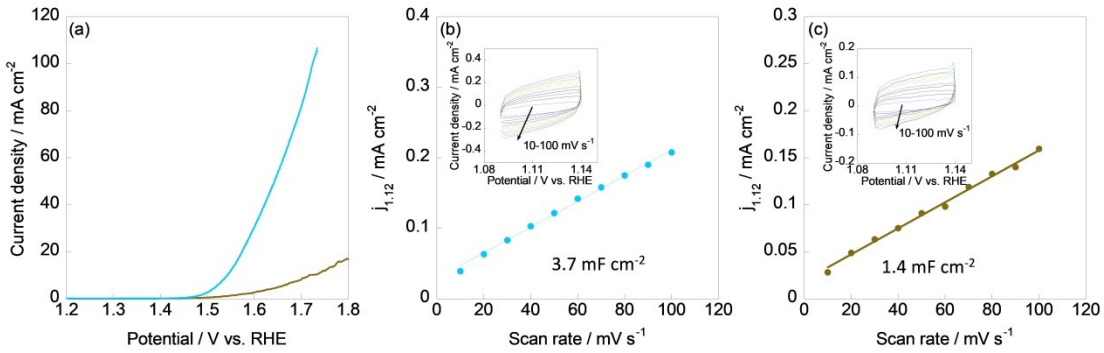

Figure S10 OER performance (a) and cyclic voltammetry curves (b, c) of commercial IrO_2 before and after 1000 cycles.

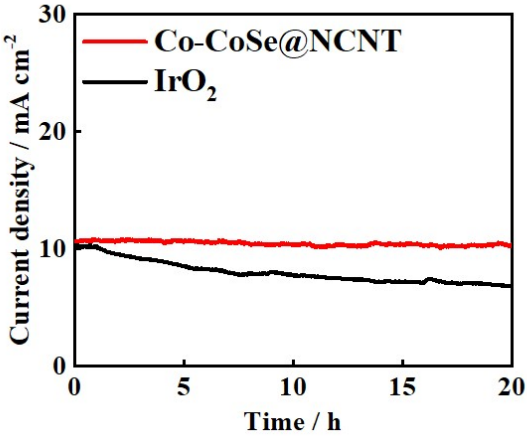

Figure S11 i-t test of IrO_2 and Co-CoSe@NCNT.

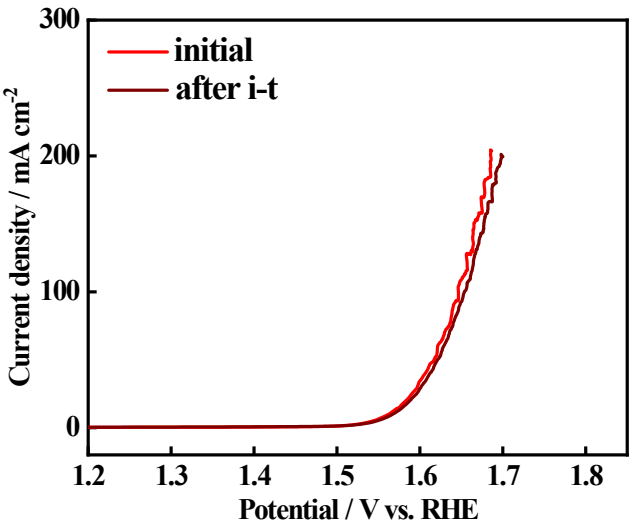

Figure S12 OER performance of Co-CoSe@NCNT electrocatalyst before and after i-t test.

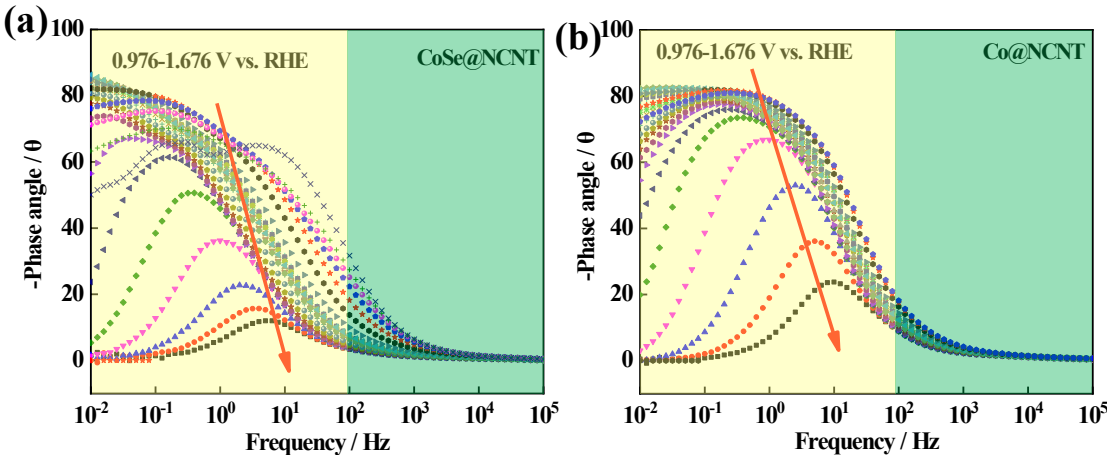

Figure S13 *in-situ* electrochemical impedance spectroscopies of Co@NCNT, CoSe@NCNT.

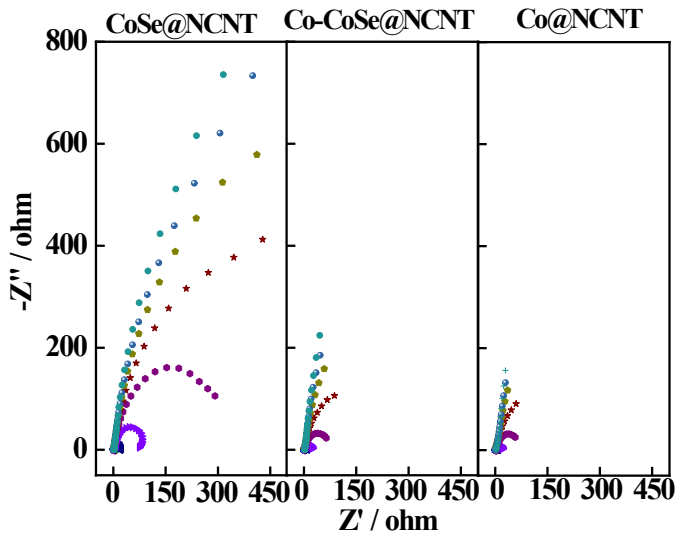

Figure S14 Electrochemical impedance spectroscopies of Co@NCNT (a), CoSe@NCNT (b) and Co-CoSe@NCNT (c).

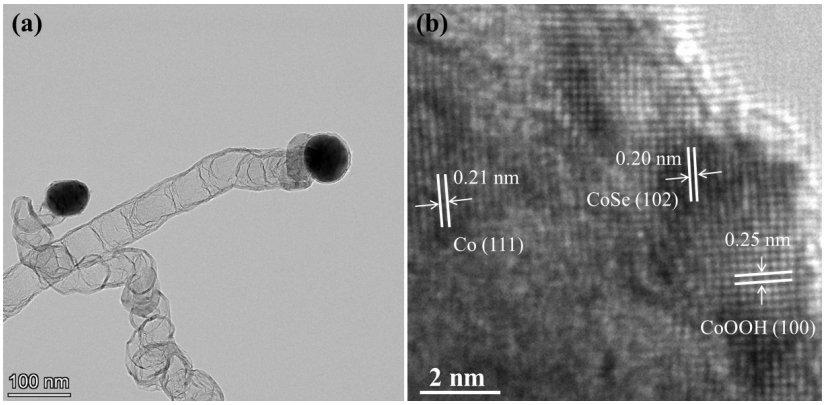

Figure S15 HR-TEM image of Co-CoSe@NCNT after OER test.

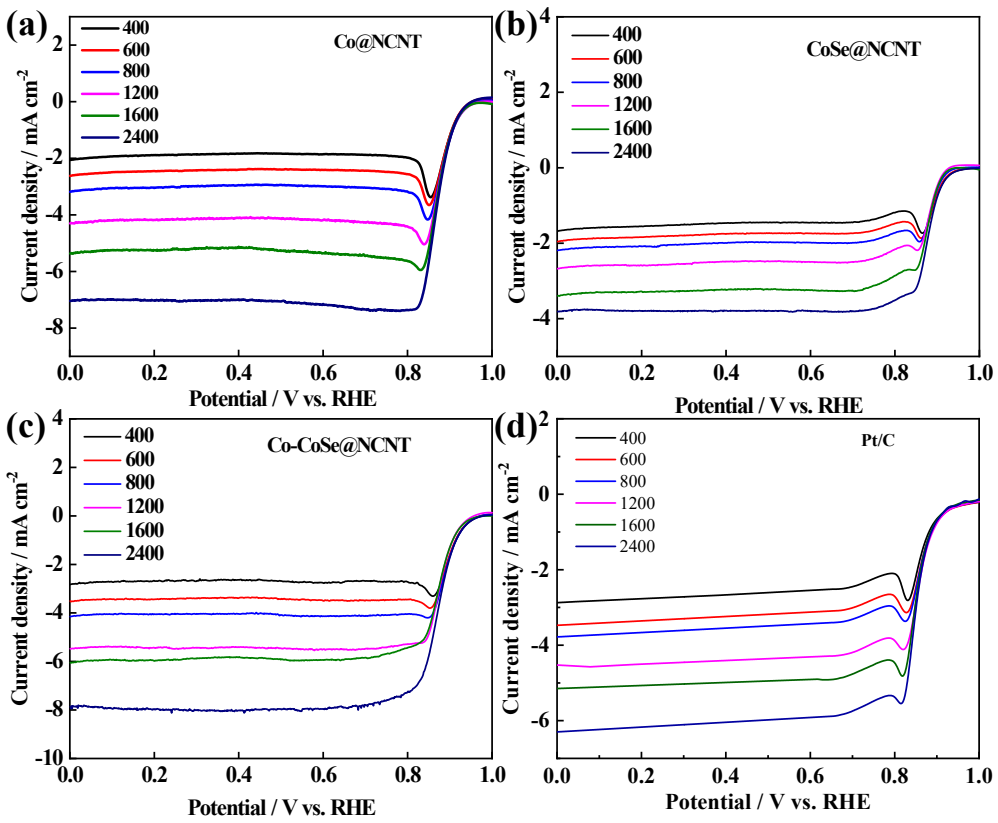

Figure S16 ORR polarization curves of Co@NCNT (a), CoSe@NCNT (b), Co-CoSe@NCNT (c) and Pt/C (d).

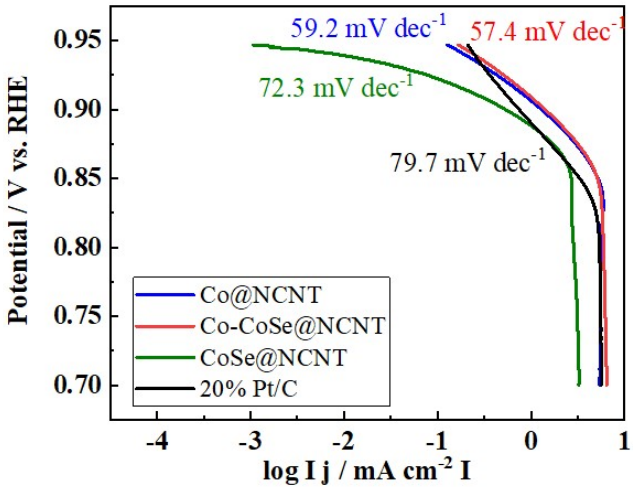

Figure S17 Tafel slope of Co@NCNT, CoSe@NCNT, Co-CoSe@NCNT and Pt/C.

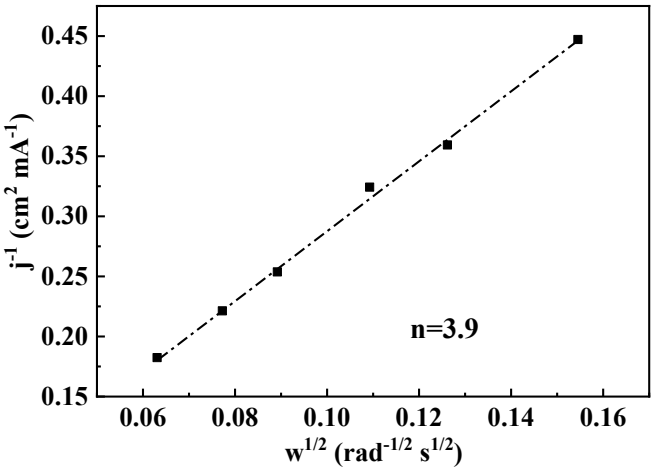

Figure S18 Koutecky-Levich equation of commercial Pt/C.

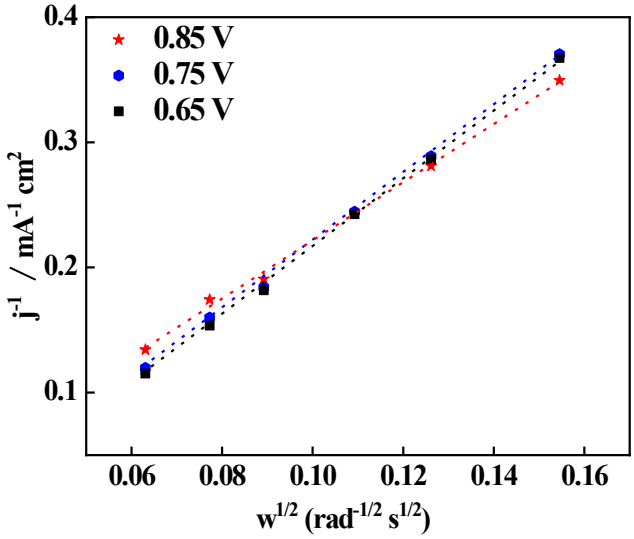

Figure S19 Koutecky-Levich equation of Co-CoSe@NCNT at various potentials.

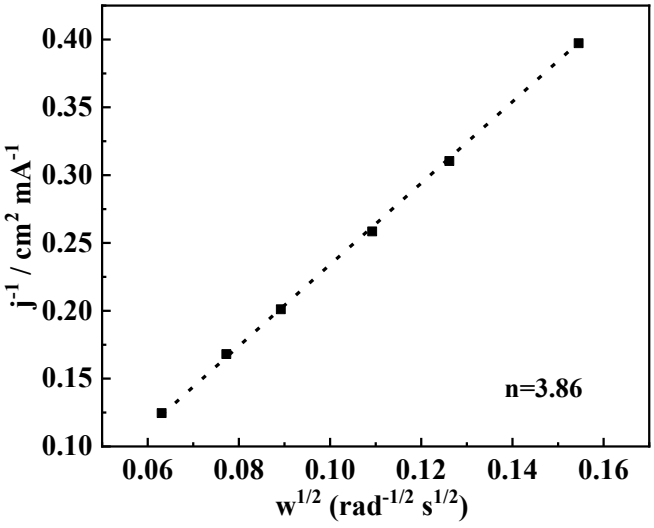

Figure S20 Koutecky-Levich equation of Co-CoSe@NCNT after 5000 cycles.

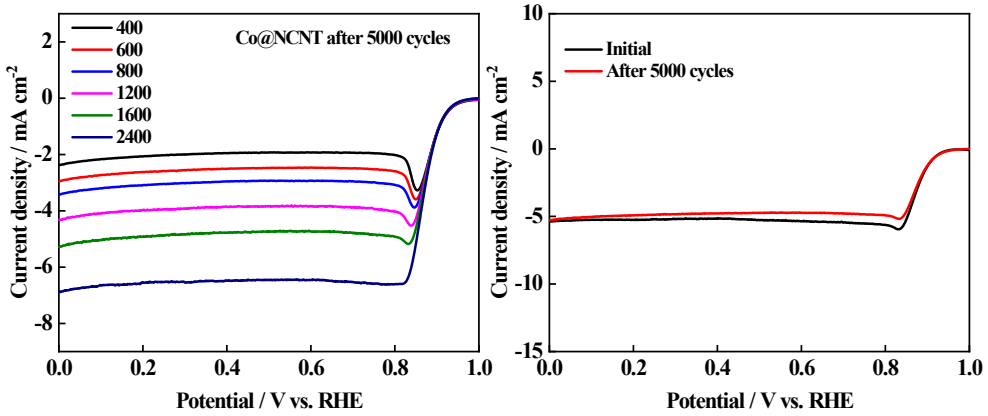

Figure S21 ORR polarization curves of Co@NCNT after 5000 cycles.

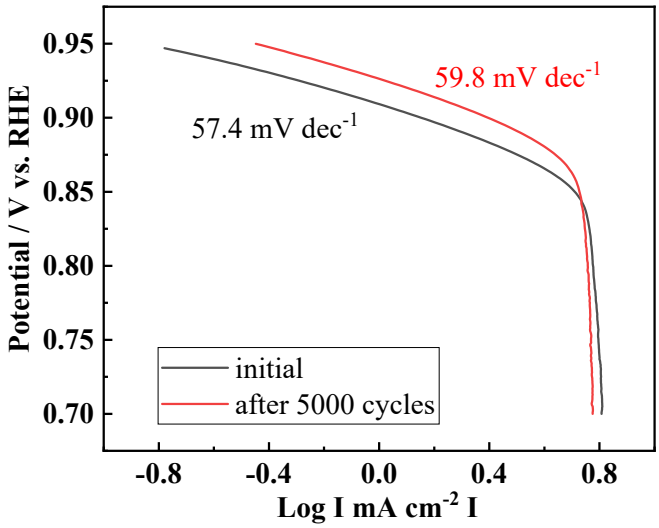

Figure S22 Tafel slope of Co-CoSe@NCNT before and after 5000 cycles.

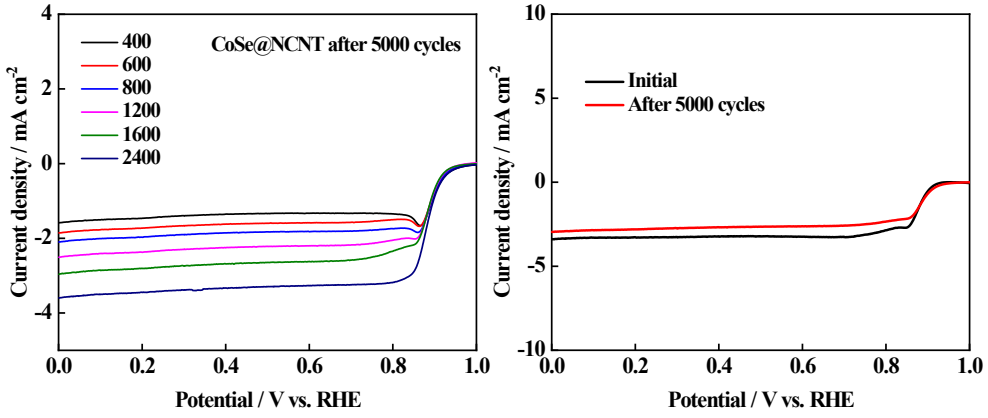

Figure S23 ORR polarization curves of CoSe@NCNT after 5000 cycles.

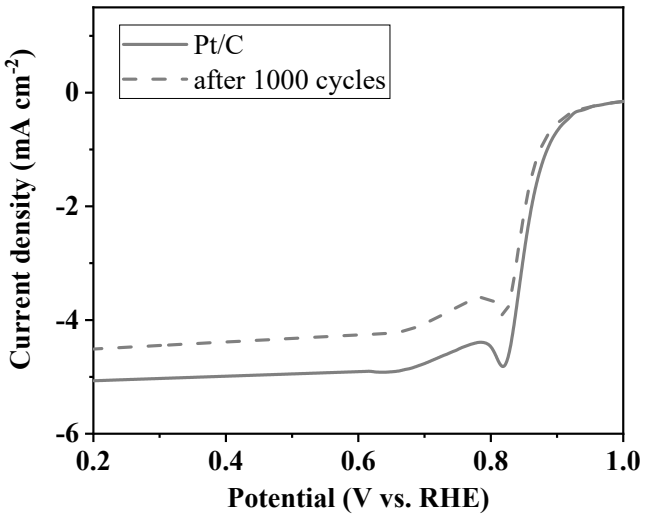

Figure S24 ORR performance of commercial Pt/C after 1000 cycles.

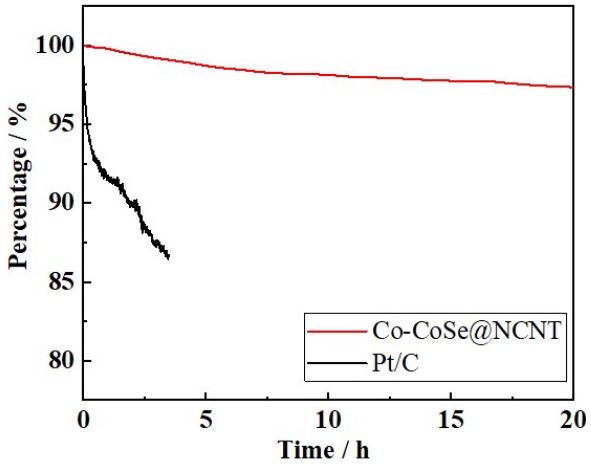

Figure S25 i-t test of Co-CoSe@NCNT and commercial Pt/C.

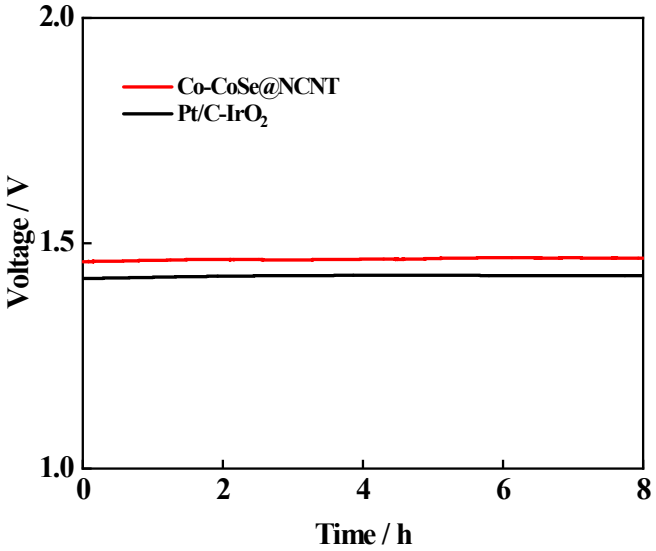

Figure S26 Open circuit voltage of Pt/C-IrO_2 and Co-CoSe@NCNT.

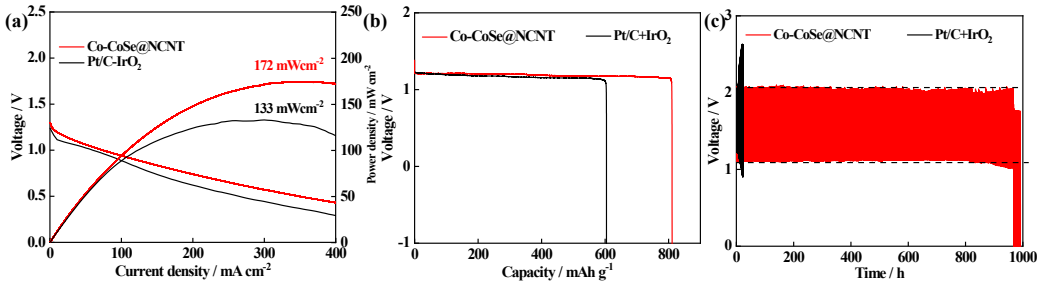

Figure S27 I-V curves (a), specific activity (b), stability test of Pt/C-IrO_2 and Co-CoSe@NCNT in aqueous R-ZABs.

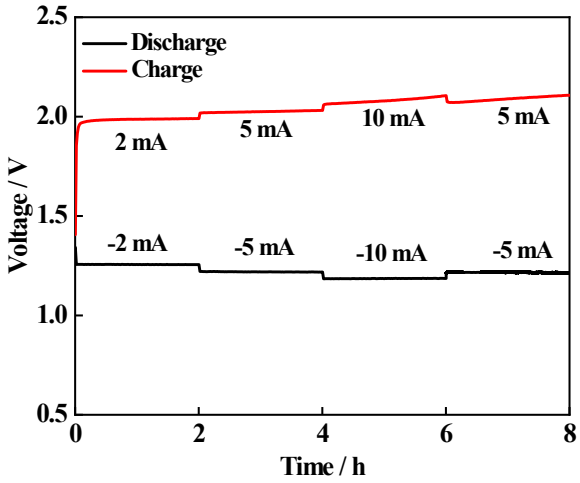

Figure S28 Charge-discharge process of Co-CoSe@NCNT at various current density.

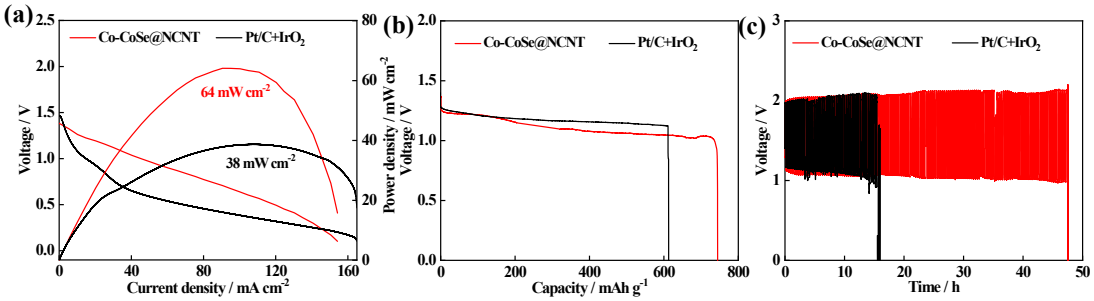

Figure S29 I-V curves (a), specific activity (b), stability test of Pt/C-IrO_2 and Co-CoSe@NCNT in all-solid-state R-ZABs.

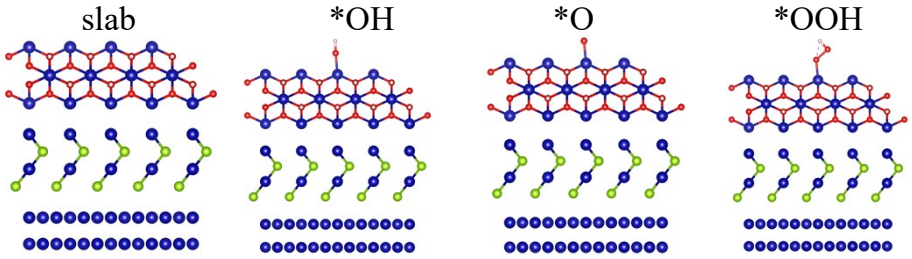

Figure S30 Chemical structures of oxygen reaction intermediates on Co-CoSe-CoOOH.

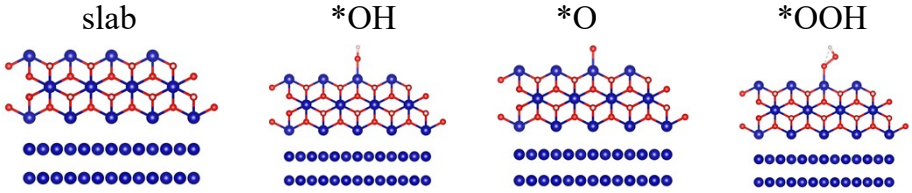

Figure S31 Chemical structures of oxygen reaction intermediates on Co-CoOOH.

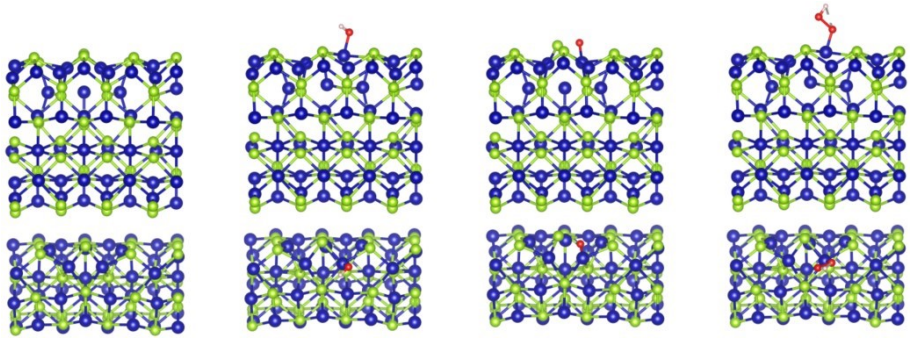

Figure S32 Chemical structures of oxygen reaction intermediates on CoSe and Co-CoSe.

References

1. Y. H. Tian, L. Xu, J. C. Qian, J. Bao, C. Yan, H. N. Li, H. M. Li and S. Q. Zhang, *Carbon*, 2019, **146**, 763-771.
2. Y. Chen, C. Gong, Z. Shi, D. Chen, X. Chen, Q. Zhang, B. Pang, J. Feng, L. Yu and L. Dong, *Journal of Colloid and Interface Science*, 2021, **596**, 206-214.
3. D. Chen, X. Chen, Z. Cui, G. Li, B. Han, Q. Zhang, J. Sui, H. Dong, J. Yu, L. Yu and L. Dong, *Chemical Engineering Journal*, 2020, **399**.
4. X. L. Guo, X. L. Hu, D. Wu, C. Jing, W. Liu, Z. L. Ren, Q. N. Zhao, X. P. Jiang, C. H. Xu, Y. X. Zhang and N. Hu, *Acs Applied Materials & Interfaces*, 2019, **11**, 21506-21514.
5. Y. X. Wang, R. J. Liu, W. D. Chen, W. M. Li, W. Zheng, H. Zhang and Z. Y.

Zhang, *Acs Sustainable Chemistry & Engineering*, 2022, **10**, 14486-14494.
6. X. H. He, J. Fu, M. Y. Niu, P. F. Liu, Q. Zhang, Z. Y. Bai and L. Yang, *Electrochimica Acta*, 2022, **413**.
7. M. H. Wang, S. Ji, H. Wang, V. Linkov, X. Y. Wang and R. F. Wang, *Journal of Power Sources*, 2023, **571**.
8. M. Moloudi, A. Noori, M. S. Rahmanifar, Y. Shabangoli, M. F. El-Kady, N. B. Mohamed, R. B. Kaner and M. F. Mousavi, *Advanced Energy Materials*, 2022, DOI: 10.1002/aenm.202203002.
9. M. M. Yin, H. Miao, J. X. Dang, B. Chen, J. Q. Zou, G. M. Chen and H. Li, *Journal of Power Sources*, 2022, **545**.
10. J. Zhou, T. Liu, J. Zhang, L. Zhao, W. He and Y. Wang, *Separation and Purification Technology*, 2023, **304**.
11. L. Wan, P. C. Wang, Y. Q. Lin and B. G. Wang, *Journal of the Electrochemical Society*, 2019, **166**, A3409-A3415.
12. T. T. Wan, H. Y. Wang, L. L. Wu, C. C. Wu, Z. S. Zhang, S. M. Liu, J. Fu and J. D. Li, *Journal of Colloid and Interface Science*, 2023, **651**, 27-35.